Update the MUSIG model in ANSYS CFX for reliable modelling of bubble coalescence and breakup

Liao, Y.;

Originally published:

January 2020

Applied Mathematical Modelling 81(2020), 506-521

DOI: https://doi.org/10.1016/j.apm.2020.01.033

Perma-Link to Publication Repository of HZDR:

https://www.hzdr.de/publications/Publ-29721

Update the MUSIG model in ANSYS CFX for reliable modelling of bubble coalescence and breakup

Yixiang Liao

Helmholtz-Zentrum Dresden - Rossendorf, Institute of Fluid Dynamics, Dresden, Germany

Abstract

The MUSIG (Multiple Size Group) model in the commercial CFD code ANSYS CFX is a population balance approach for describing binary bubble coalescence and breakup events. It is widely used in the simulation of poly-dispersed bubble flows. The purpose of this work is to identify some inconsistencies in the discrete method that applied for the solution of the population balance equation in MUSIG, and propose an improved one for discretising the source and sink terms that result from bubble coalescence and breakup. The new formulation is superior to the existing ones in preserving both mass and number density of bubbles, allowing arbitrary discretisation schemes and free of costly numerical integrations. The numerical results on the evolution of bubble size distributions in bubble flows reveal that the inconsistency in the original MUSIG regarding bubble breakup is non-negligible in both academic and practical cases. The updates presented in this work are necessary and important for calibration of bubble coalescence and breakup models using the MUSIG approach.

1 Introduction

Bubble flow normally occurs at low flow rate or holdup of the gas phase. It is widely encountered in various industrial systems like chemical, pharmaceutical and metallurgical ones because of their capability of providing large interfacial area for heat and mass transfer. In most applications, the size of bubbles takes a distribution instead of single value, and the distribution changes continuously because of various dynamic processes such as coalescence and breakup. Therefore, predicting the bubble size reliably (or interfacial area density) is a key step in the CFD modelling of bubble flows. It has been a subject of many research studies, e.g. Sun et al. (2004), Chen et al. (2004), Cheung et al. (2007), Liao et al. (2015) and Metzger and Kind (2017) among others. In most of the work, the two-fluid framework is combined with a population balance model (PBM). The population balance is a well-established method for studying coalescence (breakup) or other effects that influence the mean bubble size. By considering bubble source or sink terms caused by coalescence and breakup, the population balance equation (PBE) based on the conservation of bubble number density (Ramkrishna, 1985; 2000; Jakobsen, 2008) is formulated as:

$$\frac{\partial n\left(\vec{x},\vec{m},t\right)}{\partial t}+\nabla_{\vec{x}}\cdot\left(\dot{\vec{x}}\,n\right)+\nabla_{\vec{m}}\left(\dot{\vec{m}}\,n\right)=B_{\mathrm{C}}\left(m\right)-D_{\mathrm{C}}\left(m\right)+B_{\mathrm{B}}\left(m\right)-D_{\mathrm{B}}\left(m\right), \tag{1}$$

where n denotes the number density of bubbles, $\vec{m}$ the property space (or internal coordinate); $\vec{x}$ the physical space and t the time. The symbol $\dot{\vec{x}}$ represents the time change rate of bubble physical position. $\dot{\vec{m}}$ is the time change rate of bubble property state and plays a role in case of mass transfer. It is omitted in the following text, since it is irrelevant to the coalescence and

breakup phenomena investigated in this work. Furthermore, the present paper focuses on the univariate PBE, which has only one internal coordinate, hereafter the bubble mass m used (can also be volume or diameter), i.e. $\vec{m} = m$. On the right hand side of Eq. (1), the terms B_C, D_C, B_B, and D_B respectively represent the birth rate of bubbles with mass m due to coalescence of smaller bubbles, their death rate due to coalescence with other bubbles, birth rate due to breakup of larger bubbles, and death rate due to breakup into smaller bubbles. Like n all these terms are a function of bubble mass, time and location. For brevity, only the dependence on bubble mass m is shown in the following expressions. The source and sink terms resulting from coalescence and breakup are nonlinear and integral, which is a key feature of the PBE. In case of binary interactions, i.e. two bubbles coalescing into a new one and one bubble (parent) breaking up into two new ones (daughters), they are expressed classically as follows for a continuous m coordinate (Ramkrishna, 1985):

$$B_C(m) = \frac{1}{2}\int_0^m n(m-m')\ Q(m-m';m')\ n(m')\ dm', \tag{2}$$

$$D_C(m) = \int_0^\infty n(m)\ Q(m;m')\ n(m')\ dm', \tag{3}$$

$$B_B(m) = \int_m^\infty n(m')\ \Omega(m')\beta(m';m)\ dm', \tag{4}$$

$$D_B(m) = n(m)\ \Omega(m). \tag{5}$$

Wherein Q, Ω and β are often referred to as kernel functions. $Q(m'; m)$ denotes the coalescence frequency of a bubble of mass m with a bubble of mass m' per unit control volume. $\Omega(m')$ represents the overall breakup frequency of a parent bubble of mass m', while $\beta(m'; m)$ is the daughter size distribution function expressing the probability of a daughter bubble having mass m generated at the breakage of the parent bubble m'. Since no mass is created or dissipated during the breakup of a bubble, $\beta(m'; m)$ should satisfy

$$\int_0^{m'} m\ \beta(m';m)dm = m'. \tag{6}$$

For binary breakage, it fulfils the following constraints additionally:

$$\int_0^{m'} \beta(m';m)dm = 2, \tag{7}$$

$$\beta(m';m) = \beta(m';m'-m). \tag{8}$$

In the past great efforts have been invested in developing phenomenological kernel functions for the description of bubble coalescence and breakup in bubbly flows (Liao & Lucas, 2009;

2010). Since input parameters for these models are usually related to hydrodynamics in the flow field, e.g. turbulence eddy dissipation, numerical solution of the PBE incorporated with three-dimensional CFD calculations is often necessary for the validation of the kernel functions. On the other hand, the predictive ability of CFD simulations is largely improved by combining with a population balance model, since the spatial and temporal variation of bubble size as well as its impact on local flow fields is accounted for. In the CFD-PBM coupled simulation of bubble flows efficient solution of the PBE is of great interest. In comparison to huge efforts invested in the development and validation of coalescence and breakup models and CFD methodology, little attention has been paid to the numerical solution of the PBE. A discussion on various numerical approaches that have been used in solving the PBE was given by Bayraktar (2014). In comparison to Monte-Carlo methods and methods of moments, the method of classes with fixed pivots is the most widely-used approach, which is presented in Kumar and Ramkrishna (1996) in detail. As the name suggests, in the method of classes the bubble number density function *n* is discretized to a number of classes or bins along the mass coordinate *m*, see Fig. 1, and a PBE is solved for each class. The MUSIG (Multiple Size Group) model that investigated in this work is one variant of this method, which will be introduced in more detail below. As already discussed in some works such as Kumar and Ramkrishna (1996), Hagesaether (2002), Bove (2005) and Liao et al. (2018), discretizing Eq. (1) in the internal coordinate space (here m) with preservation of both mass and number of bubbles is not a trivial matter. Bubbles generated in a coalescence or breakup event often possess a mass different from the pivots if an arbitrarily irregular grid is applied. In this case, the resultant bubbles have to be allocated to the nearest classes appropriately so that both the mass and number is preserved. The purpose of this work is to show that the current MUSIG model in the commercial CFD code of ANSYS CFX preserves only the mass not the number of bubbles by handling the bubble coalescence and breakup terms, and thereby leads to some inconsistencies in the prediction of bubble size distribution. A formulation preserving not only the mass but also the number for binary events is proposed. The work is of importance for the calibration and development of bubble coalescence and breakup models, and contributes to reliable CFD-PBM coupled simulation of bubble flows.

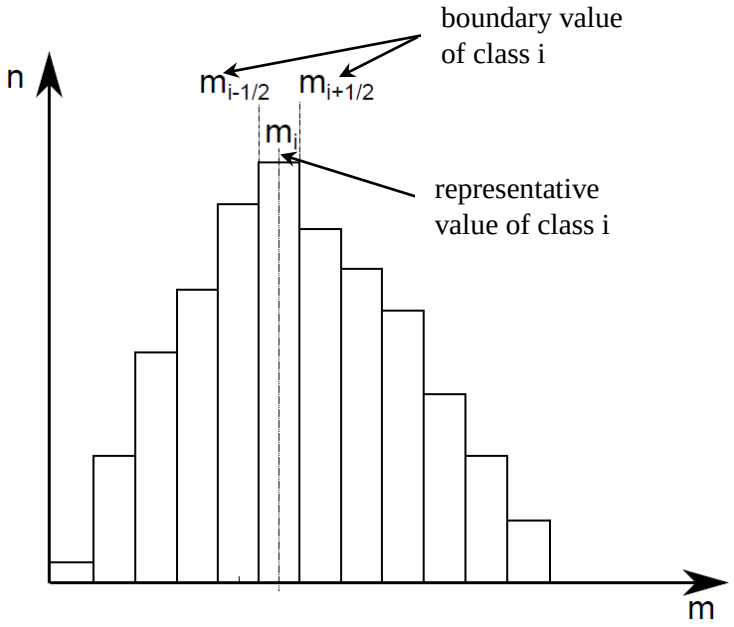

Fig. 1 Discretization of the number density function

The paper is outlined as follows: The original MUSIG model in ANSYS CFX as well as its deficiencies is presented in Section 2. Updating of the MUSIG model based on the previous work of Liao et al. (2018) is given in Section 3. In Section 4 the updated model is validated against analytical solutions for a pure coalescence and a pure breakup case, respectively. Section 5 presents the simulation results for vertical pipe flows under practical conditions using the original and the updated model. Finally, the conclusion of the work is summarized in Section 6.

2 The original MUSIG model and inconsistencies

As mentioned above the MUSIG model in ANSYS CFX is a population balance framework handling poly-dispersed multiphase flows, which is firstly proposed by Lo (2000), and then extended by Krepper et al. (2008) to consider the poly-dispersity in bubble velocities and by Lucas et al. (2011) to include mass transfer due to condensation and evaporation. The solution of the PBE is based on the method of classes introduced above. The model has been widely used for poly-dispersed bubble and droplet flows, for example

- by Cheung et al. (2007; 2013), Dorao et al. (2008), Guillen et al. (2009), Deju (2014), Liao et al. (2015) for isothermal vertical pipe flows;
- by Yeoh and Tu (2004), Krepper and Rzehak (2014) for sub-cooled wall boiling;
- by Lifante et al. (2010), Liao et al. (2014), Liao and Lucas (2016) for condensing steam-water flow;
- by Darwish and Moukalled (2008) for droplets evaporating in supersonic steam, and
- by Min et al. (2008) for aerated stirred reactors, etc.

In the previous work, deviation between simulated and measured bubble sizes routinely is attributed to the coalescence and breakup kernels or uncertainties in their input parameters. Little attention was paid to the discrete formulation of the population balance equation applied in the MUSIG model, which will be explored in detail in this work. To keep the consistency, the derivation of the size fraction equation of the MUSIG model as well as the default discrete formulation of the source and sink terms in ANSYS CFX is introduced briefly below. By discretizing the Eq. (1) into size classes, a transport equation for the bubble number concentration in each size class N_i is obtained:

$$\frac{\partial N_\mathrm{i}}{\partial t}+\nabla_{\vec{\mathrm{x}}}\cdot\left(\dot{\vec{x}}\,N_\mathrm{i}\right)=\int_{m_{i-1/2}}^{m_{i+1/2}}B_\mathrm{C}\left(m\right)dm-\int_{m_{i-1/2}}^{m_{i+1/2}}D_\mathrm{C}\left(m\right)dm+\int_{m_{i-1/2}}^{m_{i+1/2}}B_\mathrm{B}\left(m\right)dm-\int_{m_{i-1/2}}^{m_{i+1/2}}D_\mathrm{B}\left(m\right)dm\,, \tag{9}$$

where m_i is the representative mass of the bubbles in size bin i and $m_{\mathrm{i}-1/2}$, $m_{\mathrm{i}+1/2}$ are the boundary values (see Fig.1). The number concentration, N_i, is defined as

$$N_\mathrm{i}=\int_{m_{i-1/2}}^{m_{i+1/2}}n\left(m\right)dm\,. \tag{10}$$

By multiplying Eq. (9) with m_i and after a few manipulations (e.g. by substituting $m_\mathrm{i}\,N_\mathrm{i}=\rho_\mathrm{d}\,r_\mathrm{i}$) one can obtain the size fraction equation solved by the MUSIG model

$$\frac{\partial \rho_{\mathrm{d}} r_{\mathrm{d}} f_{\mathrm{i}}}{\partial t}+\nabla_{\vec{\mathrm{x}}} \cdot\left(\dot{\vec{x}}\, \rho_{\mathrm{d}} r_{\mathrm{d}} f_{\mathrm{i}}\right)=B_{\mathrm{Ci}}-D_{\mathrm{Ci}}+B_{\mathrm{Bi}}-D_{\mathrm{Bi}}, \tag{11}$$

where ρ_{d} denotes the density of the dispersed phase, and r_{i}, r_{d} the volume fraction of the size bin i and the whole dispersed phase (all bubbles), respectively. The size fraction of the class i is defined as $f_{\mathrm{i}} = r_{\mathrm{i}}/r_{\mathrm{d}}$. According to the user guide (Ansys, 2018), the birth rate of bubbles in the size group i due to coalescence of two smaller bubbles, i.e. bubble j and k, is calculated by

$$\begin{aligned} B_{\mathrm{Ci}} &= m_{\mathrm{i}} \int_{m_{\mathrm{i-1/2}}}^{m_{\mathrm{i+1/2}}} B_{\mathrm{C}}(m)\, dm \\ &= m_{\mathrm{i}}\left(\frac{1}{2}\sum_{j\le i}\sum_{k\le i} Q\left(m_{\mathrm{j}}; m_{\mathrm{k}}\right) X_{\mathrm{jki}} N_{\mathrm{j}} N_{\mathrm{k}}\right) \\ &= \left(\rho_{\mathrm{d}} r_{\mathrm{d}}\right)^2\left(\frac{1}{2}\sum_{j\le i}\sum_{k\le i} Q\left(m_{\mathrm{j}}; m_{\mathrm{k}}\right) X_{\mathrm{jki}} \frac{f_{\mathrm{j}}}{m_{\mathrm{j}}}\frac{f_{\mathrm{k}}}{m_{\mathrm{k}}}\left(m_{\mathrm{j}}+m_{\mathrm{k}}\right)\right) \end{aligned}, \tag{12}$$

where the mass matrix X_{jki} represents the fraction of mass that goes to the group i due to the coalescence between a bubble from group j and a bubble from group k,

$$X_{\mathrm{jki}}=\begin{cases} \dfrac{\left(m_{\mathrm{j}}+m_{\mathrm{k}}\right)-m_{\mathrm{i\text{-}1}}}{m_{\mathrm{i}}-m_{\mathrm{i\text{-}1}}} & \text{if } m_{\mathrm{i\text{-}1}} \le m_{\mathrm{j}}+m_{\mathrm{k}} < m_{\mathrm{i}} \\ \dfrac{m_{\mathrm{i+1}}-\left(m_{\mathrm{j}}+m_{\mathrm{k}}\right)}{m_{\mathrm{i+1}}-m_{\mathrm{i}}} & \text{if } m_{\mathrm{i}} \le m_{\mathrm{j}}+m_{\mathrm{k}} < m_{\mathrm{i+1}} \\ 0 & \text{otherwise} \end{cases}. \tag{13}$$

By the mass allocation between the groups i and i-1 (or i+1), X_{jki} satisfies the conservation of both mass and number of bubbles. The death rate due to coalescence is

$$D_{\mathrm{Ci}}=\left(\rho_{\mathrm{d}} r_{\mathrm{d}}\right)^2\left(\sum_{j} Q\left(m_{\mathrm{i}}; m_{\mathrm{j}}\right) f_{\mathrm{i}} f_{\mathrm{j}} \frac{1}{m_{\mathrm{j}}}\right). \tag{14}$$

Similarly, the contribution of birth rate due to the breakup of larger bubbles is given by

$$
\begin{aligned}
B_{\mathrm{Bi}} &= m_{\mathrm{i}} \int_{m_{i-1/2}}^{m_{i+1/2}} B_{\mathrm{B}}(m)\, dm \\
&= m_{\mathrm{i}} \sum_{j>i} g\left(m_{\mathrm{j}}; m_{\mathrm{i}}\right) N_{\mathrm{j}} \quad , \\
&= \rho_{\mathrm{d}} r_{\mathrm{d}} \sum_{j>i} g\left(m_{\mathrm{j}}; m_{\mathrm{i}}\right) f_{\mathrm{j}}
\end{aligned}
\tag{15}
$$

and the death rate due to breakup is

$$
D_{\mathrm{Bi}} = \rho_{\mathrm{d}} r_{\mathrm{d}} \left(f_{\mathrm{i}} \sum_{j<i} g\left(m_{\mathrm{i}}; m_{\mathrm{j}}\right) \right). \tag{16}
$$

The function g in Eq. (15) and Eq. (16) is termed as partial breakup frequency by Liao et al. (2018) in order to distinguish it from the overall breakup frequency Ω in Eqs. (4) and (5). According to their definitions, the relation between the functions g, Ω and β is given as follows,

$$
g\left(m_{\mathrm{j}}; m_{\mathrm{i}}\right) = \Omega\left(m_{\mathrm{j}}\right) \beta\left(m_{\mathrm{j}}; m_{\mathrm{i}}\right) \Delta m_{\mathrm{i}}, \tag{17}
$$

and

$$
\Omega\left(m_{\mathrm{i}}\right) = \frac{1}{2} \sum_{j<i} g\left(m_{\mathrm{i}}; m_{\mathrm{j}}\right), \tag{18}
$$

where the term Δm_{i} represents the width of the class i, i.e. $\Delta m_{\mathrm{i}} = m_{\mathrm{i+1/2}} - m_{\mathrm{i-1/2}}$.

As mentioned above, the Eq. (12) to Eq. (16) are copied from the ANSYS CFX user guide (Eqs. (5-147), (5-148), (5-150), (5-151), (5-152)). Some inconsistencies in the derivation can be easily discovered if one has a close look at the equations. For example, from the second equal sign to the third one in Eq. (12) the quantity m_{i} is replaced by $m_{\mathrm{j}} + m_{\mathrm{k}}$, and similarly, in Eq. (15) m_{j} takes the place of m_{i}. Because the sum of the mass birth over all size classes is equal to the mass death, namely $m_{\mathrm{j}} + m_{\mathrm{k}}$ in coalescence and m_{j} in breakup, the substitution doesn't violate the global mass conversation, i.e.

$$
\sum_i \left(B_{\mathrm{Ci}} - D_{\mathrm{Ci}} \right) = 0, \quad \text{and} \tag{19}
$$

$$
\sum_i \left(B_{\mathrm{Bi}} - D_{\mathrm{Bi}} \right) = 0, \tag{20}
$$

is still satisfied, but the terms in individual classes are not correct. It leads to violation of the global number conservation in the binary events, namely

$$\sum_i \left(2\frac{B_{\mathrm{Ci}}}{m_{\mathrm{i}}} - \frac{D_{\mathrm{Ci}}}{m_{\mathrm{i}}} \right) = \sum_i \left(2N_{\mathrm{BCi}} - N_{\mathrm{DCi}} \right) \neq 0, \quad \text{and} \tag{21}$$

$$\sum_i \left(\frac{B_{\mathrm{Bi}}}{m_{\mathrm{i}}} - 2\frac{D_{\mathrm{Bi}}}{m_{\mathrm{i}}} \right) = \sum_i \left(N_{\mathrm{BBi}} - 2N_{\mathrm{DBi}} \right) \neq 0. \tag{22}$$

Wherein N_{BCi}, N_{DCi}, N_{BBi}, N_{DBi} denotes birth and death rate of total bubble number in class i due to coalescence and breakup, respectively. Furthermore, in the derivation of Eq. (17) the mean value theorem is applied to the daughter size distribution function. In other words, it assumes that

$$\beta\left(m_{\mathrm{j}}; m_{\mathrm{i}}\right)\Delta m_{\mathrm{i}} = \int_{m_{\mathrm{i-1/2}}}^{m_{\mathrm{i+1/2}}} \beta(m_{\mathrm{j}}; m)dm, \quad \left(m_{\mathrm{i-1/2}} \leq m_{\mathrm{i}} \leq m_{\mathrm{i+1/2}}\right) \quad . \tag{23}$$

This is only applicable in case of uniform distribution, i.e. β is a constant, or the mass of the daughter bubble m coincide with the representative value m_{i}. Otherwise, it may lead to violation of the number constraint given by Eq. (7), in other words, usually

$$\sum_{i \leq j} \beta\left(m_{\mathrm{j}}; m_{\mathrm{i}}\right)\Delta m_{\mathrm{i}} \neq \int_0^{m_{\mathrm{j}}} \beta(m_{\mathrm{j}}; m)dm = 2 \quad . \tag{24}$$

The last inconsistency is that the breakup birth rate of bubbles in class i is counted twice according to Eq. (15). Because in binary breakup events the daughter bubbles and their complementary parts are symmetrical at the half parent bubble, i.e. m_{i}=0.5m_{j}, the birth rate should be summarized either over the range $m_{\mathrm{i}} < m_{\mathrm{j}} \leq 2m_{\mathrm{i}}$ or $m_{\mathrm{j}} > 2m_{\mathrm{i}}$ but not the whole range of $m_{\mathrm{j}} > m_{\mathrm{i}}$. Correspondingly, the ½ is missing in the computation of the death rate by Eq. (16).

In contrast to the kernel functions little discussion on the uncertainties of the discretization introduced by above substitution and inconsistency in the MUSIG model is available in the literature. Recently, Liao et al. (2018) showed that the error in the breakup birth rate is significant by studying an academic case of pure breakage in a zero-dimensional model, where analytical solution is possible. The authors were therefore motivated to develop a novel discrete population balance equation for binary breakage, which preserves both the total mass and number of bubbles. The framework was successfully published in the OpenFOAM 6 released by the foundation. In this work, the MUSIG model in ANSYS CFX code is updated based on this discrete formulation of the PBE, and additional corrections are performed for the coalescence birth rate. The implementation is validated against both analytical results and laboratory experiment by means of CFD-PBE coupled simulations.

3 The updated MUSIG model and advantages

The size fraction equation remains the same as in Eq. (11), and updates are carried out merely in the computation of the birth and death rates of bubbles due to coalescence and breakup. The

correction for B_{Ci} is straightforward. As already discussed above, the term $m_j + m_k$ in the last line of Eq. (12) should be m_i, i.e.

$$
\begin{aligned}
B_{Ci}^{'} &= m_i \int_{m_{i-1/2}}^{m_{i+1/2}} B_C(m)\,dm \\
&= m_i \left(\frac{1}{2} \sum_{j \le i} \sum_{k \le i} Q(m_j; m_k) X_{jki} N_j N_k \right) \qquad , \qquad (12^{'}) \\
&= (\rho_d r_d)^2 \left(\frac{1}{2} \sum_{j \le i} \sum_{k \le i} Q(m_j; m_k) X_{jki} \frac{f_j}{m_j} \frac{f_k}{m_k} m_i \right)
\end{aligned}
$$

In contrast, the reformulation of the breakup birth rate B_{Bi} in Eq. (15) needs some manipulations. To avoid the inconsistency given in Eq. (24), either a special discretisation scheme is adopted or numerical integration of β is needed. The former example is the 2^n ratio between successive bin sizes in the Hagesather method (Hagesather et al., 2002). The latter one is the formulation proposed by Kumar and Ramkrishna (1996), where the fraction of breakage sources going to representative size bins is computed from numerical integration of β over each size bin. Both formulations are available in the commercial code ANSYS FLUENT. For more details the reader are referred to the user guide. In this work, a new formulation free of above restrictions is proposed for binary breakage. As illustrated in Fig. 2, we firstly envision that the parent bubble *j* and the smaller daughter bubble *k* have the mass coinciding with the pivots or the representative values of the classes *j* and *k*, i.e. having the mass m_j and m_k, respectively. The mass of the other daughter bubble is then fixed to $m_j - m_k$, which is larger than the half mass of the parent bubble and lies near the size class *i*.

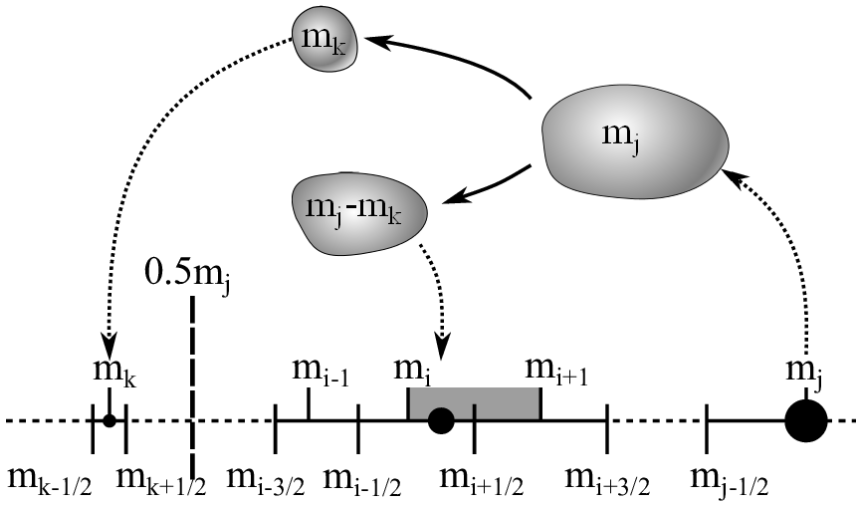

Fig. 2 schematic illustration of the discretization of bubble mass coordinate and the breakup of a bubble from class j to a bubble in class *k* and its counterpart (Liao et al., 2018)

The birth rate of the daughter bubble *k* follows directly the Eq. (15) but with the correction on the mass replacement discussed above, i.e.

$$
\begin{aligned}
B_{\mathrm{Bk}}{}' &= m_{\mathrm{k}} \int_{m_{\mathrm{k-1/2}}}^{m_{\mathrm{k+1/2}}} B_{\mathrm{B}}(m)\,dm \\
&= m_{\mathrm{k}} \sum_{j>i} g\left(m_{\mathrm{j}}; m_{\mathrm{k}}\right) N_{\mathrm{j}} \qquad , \\
&= \rho_{\mathrm{d}} r_{\mathrm{d}} \sum_{j>i} g\left(m_{\mathrm{j}}; m_{k}\right) f_{\mathrm{j}} \frac{m_{\mathrm{k}}}{m_{\mathrm{j}}}
\end{aligned}
\tag{15'}
$$

The generation of the other daughter has to be represented by the birth rates of neighbouring classes, here for example class *i*-1, *i* and *i*+1, and an appropriate allocation scheme is needed. By mimicking the mass matrix X_{jki} for coalescence given by Eq. (13), we propose a mass matrix Y_{jki} for the description of the mass fraction going to the class *i* due to the breakup of a bubble *j* to a bubble *k* (Liao et al., 2018). It is expressed as

$$
Y_{\mathrm{jki}} = \begin{cases}
\dfrac{\left(m_{\mathrm{j}} - m_{\mathrm{k}}\right) - m_{\mathrm{i-1}}}{m_{\mathrm{i}} - m_{\mathrm{i-1}}} & \text{if } \; m_{\mathrm{i-1}} \le m_{\mathrm{j}} - m_{\mathrm{k}} < m_{\mathrm{i}} \\
\dfrac{m_{\mathrm{i+1}} - \left(m_{\mathrm{j}} - m_{\mathrm{k}}\right)}{m_{\mathrm{i+1}} - m_{\mathrm{i}}} & \text{if } \; m_{\mathrm{i}} \le m_{\mathrm{j}} - m_{\mathrm{k}} < m_{\mathrm{i+1}} \\
0 & \text{otherwise}
\end{cases}
\tag{25}
$$

Furthermore, as explained by Eq. (8) the number generation rate of the two daughter bubbles is identical. The birth rate of the daughter bubble with the mass m_{j} - m_{k} can be represented by that of the daughter *k*. In this way, the constraint of number conservation given by Eq. (7) is ensured, and the error introduced by applying the mean value theorem on β as shown in Eq. (24) is avoided, since the mass of the daughter *k* coincides with the representative value. Finally, the birth rate of the bubbles in class *i* due to the generation of bubbles with m_{j} - m_{k} is computed according to

$$
\begin{aligned}
B_{\mathrm{Bi}}{}' &= m_{\mathrm{i}} \int_{m_{\mathrm{i-1/2}}}^{m_{\mathrm{i+1/2}}} B_{\mathrm{B}}(m)\,dm \\
&= m_{\mathrm{i}} \sum_{j>i} \sum_{k} g\left(m_{\mathrm{j}}; m_{\mathrm{k}}\right) Y_{\mathrm{jki}} N_{\mathrm{j}} \qquad , \\
&= \rho_{\mathrm{d}} r_{\mathrm{d}} \sum_{j>i} \sum_{k} g\left(m_{\mathrm{j}}; m_{\mathrm{k}}\right) Y_{\mathrm{jki}} f_{\mathrm{j}} \frac{m_{\mathrm{i}}}{m_{\mathrm{j}}}
\end{aligned}
\tag{26}
$$

If we consider above two situations for the size class *i*, the general expression for the birth rate due to breakup of large bubbles is given by

$$B_{\mathrm{Bi}}^{'} = \rho_{\mathrm{d}} r_{\mathrm{d}} \sum_{j>i} \frac{m_{\mathrm{i}}}{m_{\mathrm{j}}} f_{\mathrm{j}} \left(g\left(m_{\mathrm{j}}; m_{\mathrm{i}}\right) + \sum_{k<j} g\left(m_{\mathrm{j}}; m_{\mathrm{k}}\right) Y_{\mathrm{jki}} \right). \tag{27}$$

It should be noticed that in Eq. (27) $g(m_{\mathrm{j}};\ m_{\mathrm{i}})$ and $g(m_j;\ m_{\mathrm{k}})$ represents the partial breakup frequency of a bubble j to a daughter bubble i and k, respectively. Both of them are smaller than the half parent bubble mass, i.e. $m_{\mathrm{i}} < 0.5\ m_{\mathrm{j}}$ and $m_{\mathrm{k}} < 0.5\ m_{\mathrm{j}}$, since we fix the mass of the small daughter to the representative values. In the application of the formulation for binary breakage, the condition of preserving mass and number density is justified by preparing the function g using the Eq. (17) properly. Since the breakup model of Luo & Svendsen (1996) is the default one in the ANSYS CFX code, let us take it as an example to explain how to prepare $g(m_{\mathrm{j}};m_{\mathrm{i}})$ appropriately. Luo & Svendsen (1996) proposed a model for the breakup of drops and bubbles in turbulent dispersions, and it is formulated as

$$g\left(m_{\mathrm{j}};\ f_{\mathrm{bv}} m_{\mathrm{j}}\right) = 0.923 F_{\mathrm{B}} \left(1 - r_{\mathrm{d}}\right) \left(\frac{\varepsilon_{\mathrm{c}}}{d_{\mathrm{j}}^2} \right)^{1/3} \int_{\xi_{\min}}^{1} \frac{\left(1+\xi\right)^2}{\xi^{11/3}} e^{-\chi} d\xi\,, \tag{28}$$

where

$$\chi = \frac{12\left(f_{\mathrm{bv}}^{2/3} + \left(1 - f_{\mathrm{bv}}\right)^{2/3} - 1 \right)\sigma}{\beta \rho_{\mathrm{c}} \varepsilon_{\mathrm{c}}^{2/3} d_{\mathrm{i}}^{5/3} \xi^{11/3}}\,. \tag{29}$$

In Eqs. (28) and (29) the symbols ξ denotes the size ratio between an eddy and the parent particle, and f_{bv} is the volume ratio between a daughter and the parent particle, and F_{B} is an adjustable constant, $\beta = 2$, ρ_{c} and ε_{c} is the density and eddy dissipation rate of the continuous phase, and σ is the surface tension coefficient.

One should pay attention that the function $g(m_{\mathrm{j}};\ f_{\mathrm{bv}} m_{\mathrm{j}})$ in Eq. (28) is not directly the function $g(m_{\mathrm{j}};\ m_{\mathrm{i}})$ or $g(m_{\mathrm{j}};\ m_{\mathrm{k}})$ that is required for the MUSIG model. The difference seems to be overlooked in most previous work, since no related discussion is available. As described in the paper of Luo & Svendsen (1996), $g(m_{\mathrm{j}};\ f_{\mathrm{bv}} m_{\mathrm{j}})$ is related to the total breakup frequency $\Omega(m_{\mathrm{j}})$ in the following way

$$\Omega\left(m_{\mathrm{j}}\right) = \sum_{f_{\mathrm{bv}}=0}^{0.5} g\left(m_{\mathrm{j}};\ f_{\mathrm{bv}} m_{\mathrm{j}}\right) \Delta f_{\mathrm{bv}}\,. \tag{30}$$

By comparing Eq. (30) with Eq. (18) one can get

$$g\left(m_{\mathrm{j}}; m_{\mathrm{i}}\right) = g\left(m_{\mathrm{j}};\ f_{\mathrm{bv}} m_{\mathrm{j}}\right) \Delta f_{\mathrm{bv}} = g\left(m_{\mathrm{j}};\ f_{\mathrm{bv}} m_{\mathrm{j}}\right) \frac{\Delta m_{\mathrm{i}}}{m_{\mathrm{j}}}\,. \tag{31}$$

If instead of $g(m_{\mathrm{j}};\ f_{\mathrm{bv}} m_{\mathrm{j}})$, $\Omega(m_{\mathrm{j}})$ and $\beta(m_{\mathrm{j}};\ m_i)$ are provided, $g(m_{\mathrm{j}};\ m_{\mathrm{i}})$ should be derived according to Eq. (17). It is worth noting that in the new formulation the term Δm_{i} (or Δm_{k}) is not always

equal to the bin width. It should satisfy the following condition in order to ensure that $g(m_j; m_i)$ (or $g(m_j; m_k)$) refers to the breakage source of a bubble up to the half parent bubble mass, i.e. m_i (or m_k) $\leq 0.5m_j$.

$$\Delta m_i = \begin{cases} m_{i+1/2} - m_{i-1/2}, & \text{if } m_{i+1/2} \leq 0.5m_j \\ 0.5m_j - m_{i-1/2}, & \text{if } m_{i-1/2} < 0.5m_j < m_{i+1/2} \\ 0, & \text{if } 0.5m_j \leq m_{i-1/2} \end{cases}. \quad (32)$$

Finally, the Eq. (16) can be used directly to calculate the death rate of bubbles in the class *i*. Multiplication with the factor ½ is not necessary, since the breakup rate $g(m_i; m_j)$ is calculated only for $m_j \leq 0.5m_i$.

The major advantages of the updated formulation can be summarized as follows.
1) it preserves both the mass and number of bubbles;
2) it allows an arbitrary discretisation of the mass coordinate such as uniform and geometric;
3) it avoids costly numerical integrations. As indicated in the user guide of ANSYS FLUENT, if the Kumar & Ramkrishna formulation (Kumar & Ramkrishna, 1996) is chosen for the Luo & Svendsen (1996) model, the space-dependent input parameters such as turbulence dissipation rate have to be averaged over the whole domain to keep the computational time reasonable (Liao et al., 2018).

4 Validation with analytical solutions

The updated MUSIG model is implemented in ANSYS CFX through the CFX Expression Language (CEL). In the two-fluid framework it is validated firstly for two academic cases, one pure coalescence and one pure breakage, where simple kernel functions are adopted and constant flow fields are assumed. The results are compared with the analytical ones as well as those obtained using the original MUSIG model. Subsequently, they are applied in quasi two-dimensional CFD-PBE coupled simulation of vertical bubbly flows, where phenomenological models for coalescence and breakup presented by Liao et al. (2015) are used. In all the cases, the continuous phase is water and the dispersed one is air. As listed in Table 1, constant material properties are assumed.

Table 1 Material properties

ρ_c [kg/m^3]	ρ_d [kg/m^3]	σ [N/m]	μ_c [Pa·s]	μ_d [Pa·s]
997	1.18	0.072	8.899×10^{-4}	1.831×10^{-5}

4.1 Pure coalescence

Scott (1968) has presented analytical solutions for the pure coalescence case with a constant coalescence kernel, i.e. $Q = 1\ m^3/s$, and an exponential initial condition for the number density is assumed

$$n\left(m,t=0\right)=\frac{N_0}{m_0}\left(\frac{m}{m_0}\right)\exp\left(-\frac{m}{m_0}\right), \tag{33}$$

where v denotes the bubble volume, and $N_0 = 2.5$, $m_0 = 0.0118$ kg. The case has been also studied by Kumar & Ramkrishna (1996) and Liao et al. (2018) using the method of classes. For the test, a constant volume fraction of the dispersed phase is assumed, i.e. $r_d = 0.05$. The mass coordinate is discretized into 54 classes using a geometric grid ($m_{i+1} = sm_i$). The ratio s and the minimum bubble mass is set to 1.5 and 1.04×10^{-5} kg, respectively. According to Eqs. (33) and (10) the initial size fraction f_i can be calculated from the relation $f_i = N_i\, m_i / r_d \rho_d$. The computational domain is a cubic box with the top exposed to the atmosphere as described in Liao and Lucas (2018). The flow field is stagnant, and no buoyancy model is activated. It is a quasi zero-dimensional simulation. Details about the mathematical and numerical setup are provided in Table 2.

Table 2 Numerical setup for the pure coalescence case

analysis type	transient
time step	0.01s
multiphase model	homogeneous
turbulence model	laminar
heat transfer model	isothermal
convergence criteria	maximum residual $\leq 10^{-4}$
advection scheme	high resolution
transient scheme	second order backward Euler
equations solved	- mixture momentum equation - pressure equation - liquid mass equation - size fraction equations

Firstly the conservation of bubble mass and number in the computation of binary coalescence process is checked. As described in Eq. (19) and Eq. (21), the mass and number is conserved if $\sum B_{Ci}/\sum D_{Ci}=1$ and $\sum N_{BCi}/\sum N_{DCi}=0.5$ is satisfied. The results shown in Fig. 3 reveal that both the original and the updated formulations preserve the mass, but the former violates the number conservation. The ratio of $\sum N_{BCi}/\sum N_{DCi}$ is slightly larger than 0.5 according to the original MUSIG model, which means that two bubbles disappear and more than one bubble is generated. It is inconsistent with binary coalescence scenario. The updated formulation presented in this work remedies this problem, see Fig. 3(b).

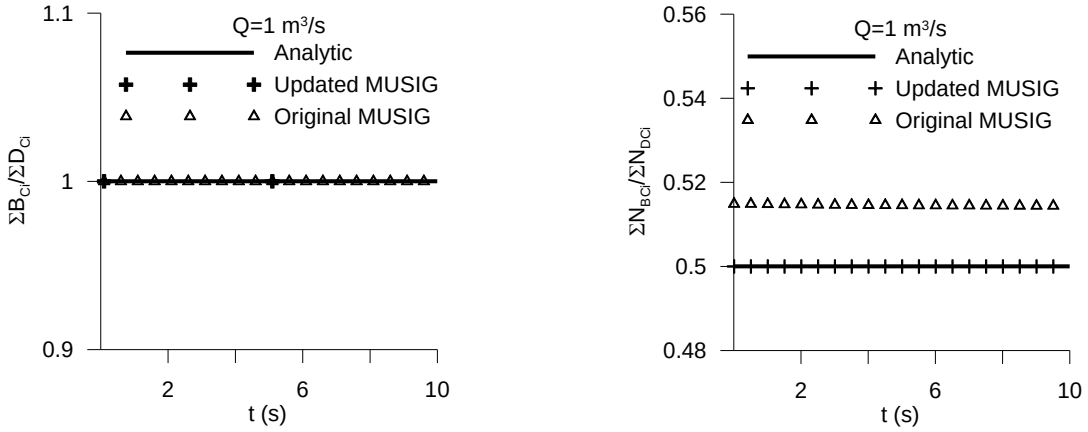

(a) mass conservation (b) number conservation

Fig. 3 Check the conservation of mass and number during binary coalescence (pure coalescence, Q = 1.0 m^3/s, mass conservation: $\sum B_{Ci}/\sum D_{Ci}=1$, number conservation: $\sum N_{BCi}/\sum N_{DCi}=0.5$)

The bubble number and size fraction density functions at t = 10 s predicted by the original and the updated MUSIG model are illustrated in Fig. 4(a) and 4(b), respectively. The dash line symbolizes the initial condition given by Eq. (33). The solid lines denotes analytical solutions, while the symbols are numerical ones. Although the difference is not dramatic, the original MUSIG model, where the mass m_i is replaced by $m_j + m_k$ during the derivation of the birth rate term B_{Ci} (see Eq. 12), leads to a clear under-prediction for small and moderate bubbles, while over-prediction at large sizes, where the number concentration is low. It implies that the coalescence rate is over-estimated. On the other hand, the numerical results obtained using the updated MUSIG model coincide with the analytical ones in the range from small to moderate bubble size. Over-predictions are observed at large bubble sizes, although they are more close to the analytical solutions than the original results. The deviation is suspected due to discretization errors. As shown by Kumar & Ramkrishna (1996), a very good agreement can be achieved in this range if a finer grid with s = 1.25 is used.

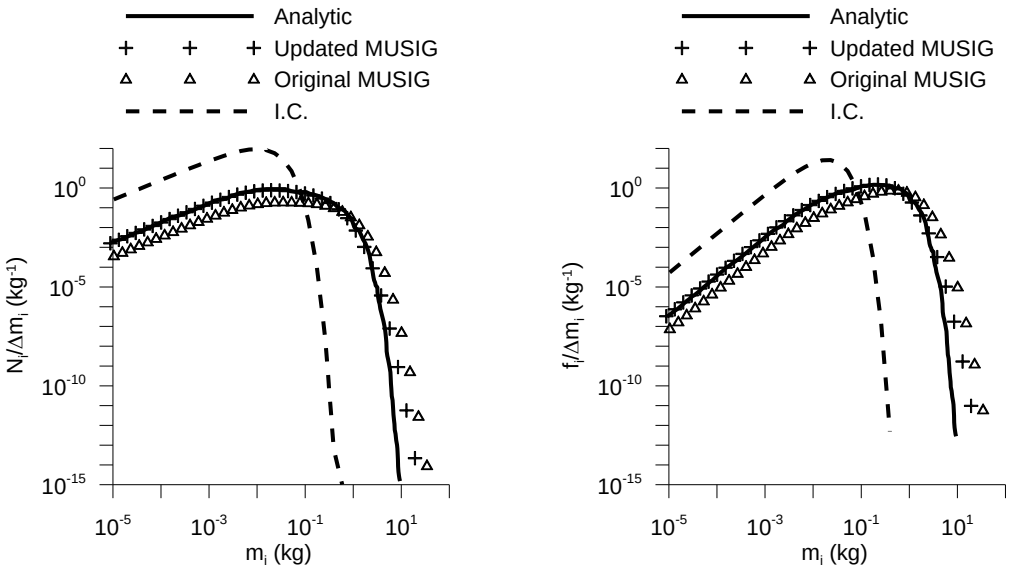

(a) number density (b) size fraction density

Fig. 4 Comparison between the numerical and analytical solutions for bubble number and size fraction density (pure coalescence, Q = 1.0 m^3/s, t = 10 s)

4.2 Pure breakage

To illustrate the necessity of the updates regarding the birth rate term B_{Bi} presented in this work, a pure breakage case with power breakup rate and uniform daughter size distribution is considered, i.e. $\Omega(m) = (m/\rho_d)^2\, m^{-6}\, s^{-1}$, $\beta(m; m') = 2.0 / m$. The computational domain, numerical and mathematical setups are identical to the above case, but with less size classes. The bubble mass coordinate begins with 1.38×10^{-5} kg and ends with 1.18 kg, and is divided into 29 bins with s = 1.5. A mono-disperse initial condition at the largest class is assumed (illustrated by the dash line in Fig. 5). Like in the coalescence case, the quantities of interest are set to be the number density and size fraction density here. The comparison between the numerical results and the analytical solution is shown in Fig. 5(a) and 5(b), respectively. One can see that in this case the original MUSIG model fails to reproduce the analytical results and gives severe over-prediction of small and moderate bubbles. In contrast, both the number and size fraction density obtained using the updated MUSIG model are in excellent agreement with the analytical solutions. It suggests that the updates regarding the breakup birth and death rate term are indispensable.

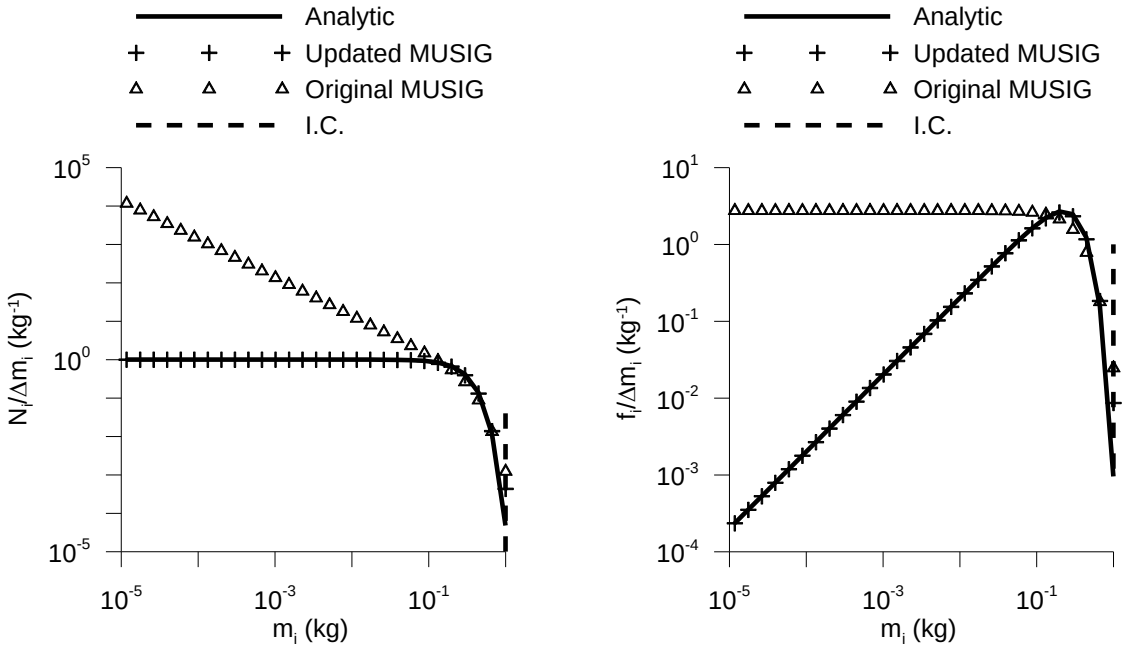

(a) number density (b) size fraction density

Fig. 5 Comparison between the numerical and analytical solutions for bubble number and size fraction density (pure breakage, $\Omega(m) = (m/\rho_d)^2\, m^{-6}\, s^{-1}$, $\beta(m;m') = 2.0/\, m$, t = 10 s)

Like in the pure coalescence case, the discrepancy observed in the original MUSIG is related to the violation of the conservation of bubble numbers. According to Eq. (22) the bubble number is preserved in binary breakage events if the ratio $\sum N_{BCi}/\sum N_{DCi}$ is equal to 2, which means that two bubbles are generated if one bubble breaks. As shown in Fig. 6(b) the original MUSIG formation obtains a too large value for $\sum N_{BCi}/\sum N_{DCi}$, while the updated one coincides with the analytic solution of 2.

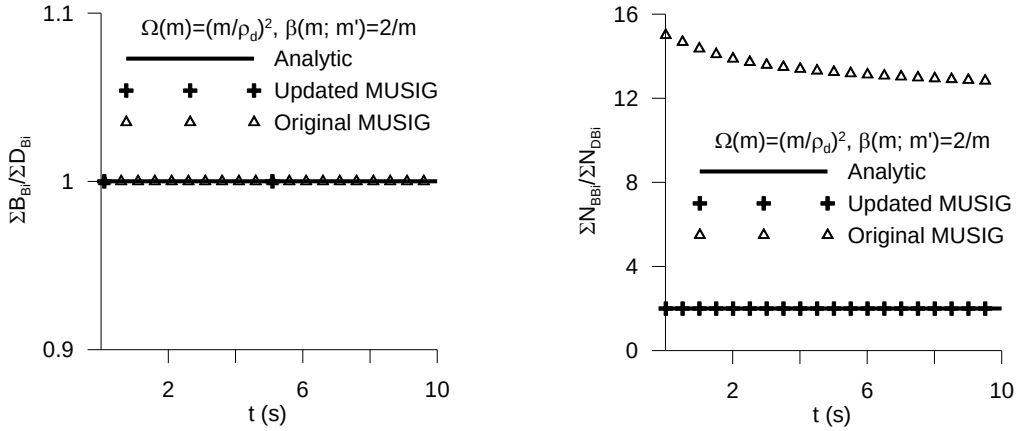

(a) mass conservation (b) number conservation

Fig. 6 Check the conservation of mass and number during binary breakup (pure breakage, $\Omega(m) = (m/\rho_d)^2\, m^{-6}\, s^{-1}$, $\beta(m;m') = 2.0/m$, mass conservation: $\sum B_{Ci}/\sum D_{Ci}=1$, number conservation: $\sum N_{BCi}/\sum N_{DCi}=2$)

5 Application for vertical pipe flows

In addition to the academic cases, four vertical pipe flow cases are simulated. In these cases simultaneous coalescence and breakup takes place, and experimental data on the change of bubble size distribution along the pipe are available.

5.1 Test cases

The validated CFD-PBM coupled model is used to predict the bubble size change in vertical pipe bubble flows. The data for comparison are taken from two stationary adiabatic air-water experiments conducted on the MTLoop and TOPFLOW facility at Helmholtz–Zentrum Dresden – Rossendorf (HZDR). The construction of the vertical pipe test section, air injection devices as well as wire-mesh sensors are illustrated in Fig. 7. In the MTLoop experiment, air was injected from 19 nozzles at the bottom, which have a diameter of 1 mm and are distributed axis symmetrically over the cross section (see Fig. 7(a)). The vertical test section has an inner diameter of 51.2 mm and a length of 3.5 m. It consists of several segments, which are connected with flanges. Sensors can be mounted in each of the flanges (Lucas et al., 2005). By combining different long segments, the distance between the gas injection and the sensor position can be varied. Table 3 shows the distance of each measurement plane to the gas injection.

Table 3 Distance between measurement plane and gas injection in MTLoop experiment

Plane	A	B	C	D	E	F	H	J	K	L
Distance [m]	0.03	0.08	0.13	0.23	0.43	0.83	1.53	2.03	2.53	3.03

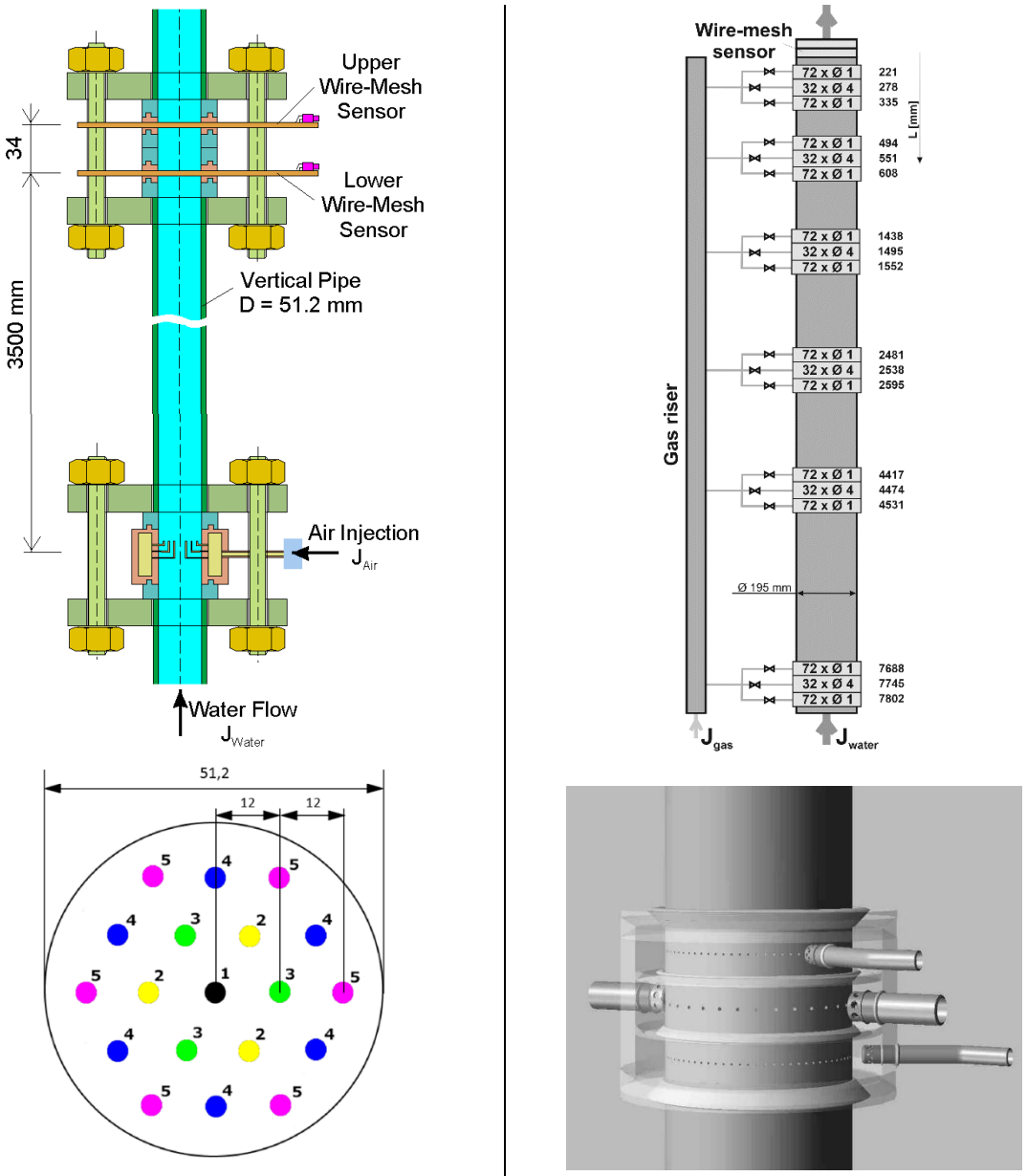

(a) MTLoop facility (b) TOPFLOW facility

Fig. 7 Test facilities for upward pipe flow experiments

The test section in the TOPFLOW experiment consists of a DN 200 pipe having a length around 8 m. The air was injected symmetrically from the pipe wall (see Fig. 7(b)) through orifices. A variable gas injection system consisting of several injection modules was designed to vary the distance between the injection position and the sensors while the sensors is fixed at the top of the pipe. The six injection modules are distributed almost logarithmically over the total height. Each of them consists of three injection chambers. The uppermost and the lowest one are provided with 72 x 1 mm orifices and the middle chambers have 32 x 4 mm orifices. The distance between measurement planes and gas injection for 1 mm and 4 mm orifices is summarized in Table 4.

Table 4 Distance between measurement plane and gas injection in TOPFLOW experiment

$D_{orifice}$= 1mm	Plane	A	C	D	F	G	I	J	L	M	O	P	R
	Distance [m]	0.221	0.335	0.494	0.608	1.438	1.552	2.481	2.595	4.417	4.531	7.688	7.802
	Plane	B	E	H	K	N	Q						

$D_{orifice}$= 4mm	Distance [m]	0.278	0.551	1.495	2.538	4.474	7.745	

In each experiment, tests were conducted for a large matrix with different combination of superficial gas and liquid velocities, and radial gas volume fraction, bubble size distribution as well as vertical gas velocity were measured with aid of two wire-mesh sensors. The data have been used frequently for model validation, e.g. Dorao et al. (2008), Krepper et al. (2008), Liao et al. (2011; 2015), Cheung et al. (2013). In this work two test cases from each experiment are simulated to show the effect of the updates in the MUSIG model on the prediction of bubble size distribution. Table 5 summarizes the experimental conditions, where J_L, J_G represents the superficial liquid and gas velocity, respectively, and $D_{orifice}$ is the orifice diameter used for gas injection.

Table 5 Experimental conditions of the investigated test cases

Experiment	Test cases	J_L [m/s]	J_G [m/s]	$D_{orifice}$ [mm]
MTLoop	063	1.017	0.0235	1.0
	074		0.0368	
TOPFLOW	063		0.0235	4.0
	074		0.0368	

Because of different gas injection methods, the initial bubble size and evolution of the distributions is obviously different in the two experiments even at identical superficial gas and liquid velocities. As shown in Fig. 8 the total evolution trend (from Level A to Level L in the MTLoop cases and from Level B to Level Q in the TOPFLOW cases) in the MTLoop cases is dominated by bubble coalescence while in the TOPFLOW ones by breakup. This is because in the TOPFLOW experiment big bubbles (5 ~ 20 mm) are present near the injection position due to the large orifices.

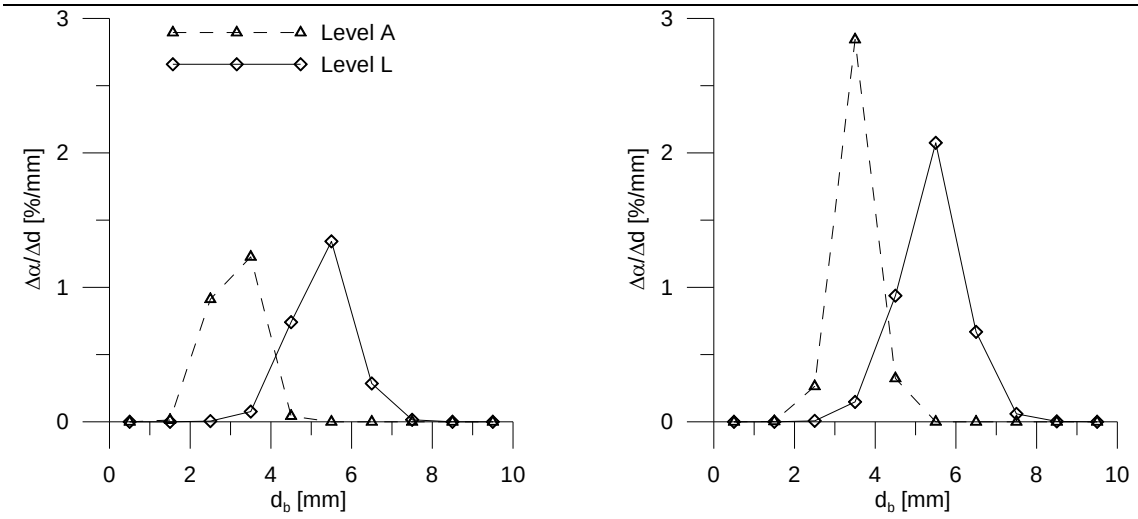

(a) MTLoop_063 (b) MTLoop_074

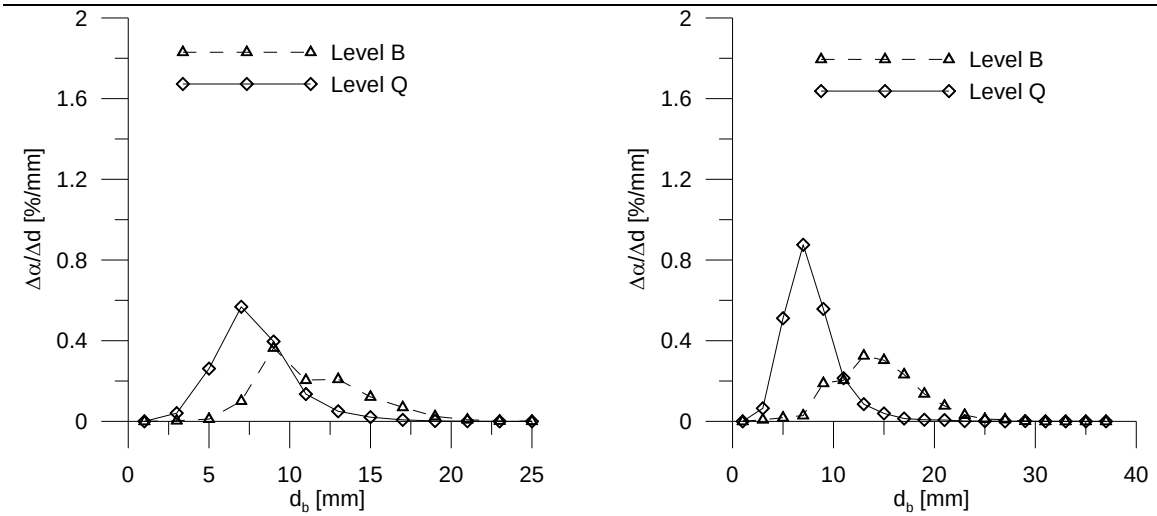

(c) TOPFLOW_063 (d) TOPFLOW_074

Fig. 8 Experimental observation of bubble size evolution along the pipe (from Level A to L, from Level B to Q)

5.2 Simulation setup

The computational domain and model is the same as that introduced in the previous work of Liao et al. (2019). Instead of the whole pipe a wedge covering 4º of the circumferences is simulated, and a quasi 2D mesh with one layer of cells in the circumferential direction is applied. The boundaries consist of inlet, outlet, symmetrical planes and wall. Measurements at the lower plane (A in MTLoop cases or B in TOPFLOW cases, see Table 4) are used as inlet conditions for the numerical analysis. The pressure boundary condition at the outlet is given as atmospheric pressure. The near-wall mesh resolution is checked by controlling the y+ value around 65 in all test cases, which is sufficiently fine for the k-ω SST model with automatic wall treatment. Closure laws for the interfacial transfer terms in the two-fluid model are specified under the guidance of the HZDR baseline strategy to avoid uncertainty related to model combination and tuning (Lucas et al., 2016). It contains specification for bubble forces, bubble coalescence and breakup and turbulence modelling, see Table 6.

Table 6 Baseline model for specifying two-fluid model closures

	Term	Model and Reference
Interfacial forces	drag	Ishii and Zuber (1979) model
	shear lift	Tomiyama et al. (2002)
	virtual mass	virtual mass coefficient set to 0.5
	wall force	Hosokawa et al. (2002)
Turbulence	liquid	k-ω SST model, Menter (1994)
	gas	dispersed phase zero equation model, $\upsilon_{td} = \upsilon_{tc}$
	BIT	Ma et al. (2017)
Bubble size	PBM	MUSIG model, Krepper et al. (2008), Liao et al. (2018)
	coalescence	Liao et al. (2015)
	breakup	Liao et al. (2015)

The forces responsible for interfacial momentum transfer consist of drag, shear lift, virtual mass and wall lubrication force. With regard to turbulence modelling the k-ω SST model with automatic wall treatment (Menter, 1994) is applied for the liquid phase, while the eddy kinematic viscosity of the gas is assumed to be equal to the liquid one. The coalescence and

breakup model presented in Liao et al. (2015) is adopted to close the birth and death terms in the MUSIG size fraction equation, i.e. Eq. (11). In turbulent bubble flow, bubble coalescence and breakup may result from various mechanisms such as turbulent fluctuation and interfacial slip. The model is generalized by accounting for all the mechanisms, whose advancement against the combination of the Prince & Blanch (1990) coalescence model and the Luo & Svendsen (1996) breakup model has been presented in Liao et al. (2015). The focus of the current work is validating the updated discrete formulation of the PBE. Coalescence and breakup due to turbulent fluctuation is considered. Like in the Luo & Svendsen (1996) model, the partial breakup frequency $g(m_j; f_{bv}m_j)$ is provided by Liao et al. (2015). For more details on the baseline model, the reader are referred to the previous work of Liao et al. (2018; 2019) as well as the references listed in Table 6.

5.3 Numerical results

The simulated and measured bubble size distribution at the top of the pipe as well as inlet is depicted in Fig. 9 for the four cases in Table 5. In accordance with the experimental data the bubble size distribution is defined as the percentage of void fraction in each class divided by the class width, i.e. $\Delta\alpha/\Delta d$. As observed in the experiment, bubble size in the cases MTLoop 063 and MTLoop 074 increases from Level A to Level L and the distribution shifts to the right. It implies that in these simultaneous coalescence and breakup cases coalescence is dominant. The coalescence and breakup model is capable of capturing this trend, but difference is present between the predictions obtained using the default and improved MUSIG frameworks. The default one in ANSYS CFX is prone to under-predict the bubble size because of over-prediction of the breakup rate as discussed in the pure breakup case. The updated formulation presented in this work improves the results considerably, and the predicted bubble size distribution conforms to the measured one. The improvement is even significant in the two TOPFLOW cases, where the evolution is dominated by bubble breakage. As shown in Fig. 9(c) the bubble size at Level B ranges from 5 to 20 mm and has a Sauter mean diameter around 10 mm. Due to the effect of breakage bubble size decreases, and the mean diameter reduces to 7 mm at Level Q. Again, the breakup-dominant trend is captured well by the coalescence and breakup model of Liao et al. (2015). The difference between the numerical results comes exclusively from the discrete formulation of the death and birth terms in the population balance equation. The default formulation provided by the ANSYS CFX code obviously delivers a too large breakup rate. One should be aware of this inconsistency if we are calibrating the coalescence and breakup models on basis of this formulation. The initial bubble size is slightly larger in case TOPFLOW 074 because of a higher superficial gas velocity. Otherwise, the evolution of bubble size distribution is similar to that in TOPFLOW 063, and dominated by breakup. In both cases, the bubble size distribution predicted by the coalescence and breakup model of Liao et al. (2015) using the updated MUSIG framework proposed in this work agrees quantitatively with the measurement. The necessity of the updating is evidenced in both academic and real bubble flow cases, especially in pure breakup and breakup-dominant cases.

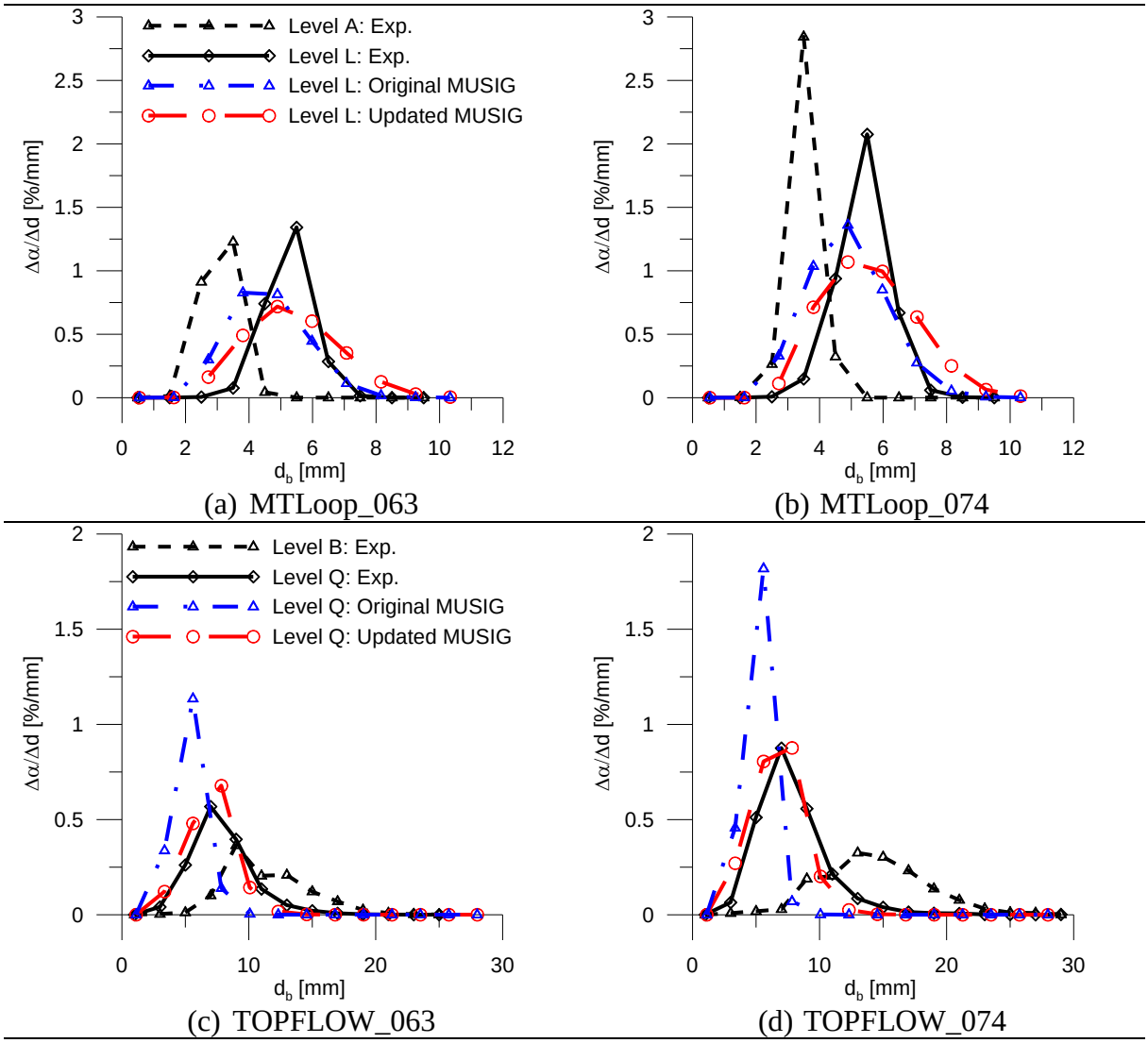

Fig. 9 Comparison between the simulated and measured bubble size distribution at the top of the pipe (Level L or Level Q)

6 Conclusion

Modelling of poly-disperse bubble flow by means of the CFD-PBM coupled method has received great attention. There have been numerous efforts to improve bubble coalescence and breakup kernels while discussion on numerical discretisation of the PBE itself is scarce. The method of classes discussed in this work is an attractive and widely used approach, which however may lead to inconsistency regarding the conservation of bubble number when breakup events are considered. Although it is aware for some researchers, a robust and efficient discrete formulation of the PBE for breakup is not available. The existing formulations in the commercial CFD codes such as ANSYS CFX and FLUENT either preserve only the mass or have restriction on discretisation schemes or rely on costly numerical integrations. Recently, Liao et al. (2018) proposed a discrete formation for accounting for binary breakage. It overcomes the limitations in existing formulations in the commercial codes, and may facilitate efficient combination with the CFD methodology. The formulation was validated in a standalone way in OpenFOAM, and the flow parameters were assumed constant. In the present work, the inconsistencies in the original MUSIG model in ANSYS CFX are discussed basing on the user's guide, and corresponding updates are carried out. The updated formulation is

validated against analytical results for two academic cases and experimental data for four laboratory pipe flow cases. In the academic cases the flow parameters are assumed constant, while in the pipe flow ones CFD-PBM coupled simulations are performed. The results evidence the success and necessity of the updates in both cases. The work is meaningful in warning the users of the inconsistencies in the commercial code, and assisting the development of bubble coalescence and breakup kernels.

References

Ansys, 2018. ANSYS CFX-solver theory guide, release 19.2. Canonsburg: Ansys, Inc.

Bayraktar, E., (2014). Numerical aspects of population balance equations coupled to computational fluid dynamics. *PhD thesis*, Technical University of Dortmund.

Bove, S., Solberg, T., Hjertager, B.H., (2005). A novel algorithm for solving population balance equations: the parallel parent and daughter classes: Derivation, analysis and testing. *Chemical Engineering Science*, **60**, 1449-1464.

Chen, P., Sanyal, J., Dudukovic, M.P., (2004). CFD modeling of bubble columns flows: implementation of population balance. *Chemical Engineering Science*, **59**, 5201-5207.

Cheung, S.C.P., Yeoh, G.H., Tu, J.Y., (2007). On the numerical study of isothermal vertical bubbly flow using two population balance approaches. *Chemical Engineering Science*, **62**, 4659-4674.

Cheung, S.C.P., Deju, L., Yeoh, G.H., Tu, J.Y. (2013). Modeling of bubble size distribution in isothermal gas-liquid flows: Numerical assessment of population balance approaches. *Nuclear Engineering and Design*, **265**, 120-136.

Darwish, M., Moukalled, F., (2008). Comparison of supersonic droplet mixing and evaporation between the multiphase, MUSIG and H-MUSIG models. *6th International Conference on CFD in Oil & Gas, Metallurgical and Process Industries*, SINTEF/NTNU, Trondheim Norway, 10-12 June 2008.

Deju, L., (2014). Population balance modelling of gas-liquid bubbly flow: capturing coalescence and breakup processes. *PhD thesis*, RMIT University.

Dorao, C.A., Lucas, D., Jakobsen, H.A., (2008). Prediction of the evolution of the dispersed phase in bubbly flow problems. *Applied Mathematical Modelling*, **32**, 1813-1833.

Guillen, D.P., Shelley, J.K., Antal, S.P., Tselishcheva, E.A., Podowski, M.Z., Lucas, D., Beyer, M., (2009). Optimization of a two-fluid hydrodynamic model of churn-turbulent flows. *17th International Conference on Nuclear Engineering*, ICONE17, July 12-16, 2009, Brussels, Belgium.

Hagesaether, L., (2002). Coalescence and break-up of drops and bubbles. *PhD thesis*, Norwegian University of Science and Technology.

Hosokawa, S., Tomiyama, A., Misaki, S., Hamada, T., (2002). Lateral migration of single bubbles due to the presence of wall. *Proceedings of ASME FEDSM'02, ASME 2002 Fluids Engineering Division Summer Meeting*, Montreal, Quebec, Canada, July 14-18, 2002

Ishii, M., Zuber, N., (1979). Drag coefficient and relative velocity in bubbly, droplet or particulate flows. *AIChE Journal*, **25**, 843-855.

Jakobsen, H.A., 2008. Chemical reactor modeling: Multiphase reactive flows. Springer-Verlag Berlin Heidelberg.

Krepper, E., Lucas, D., Frank, T., Prasser, H.-M., Zwart, P.J., (2008). The inhomogeneous MUSIG model for the simulation of polydispersed flows. *Nuclear Engineering and Design*, **238**, 1690-1702.

Krepper, E., Rzehak, R., (2014). CFD for subcooled flow boiling: Analysis of DEBORA tests. *The Journal of Computational Multiphase Flows*, **6**, 329-359.

Kumar, S., Ramkrishna, D., (1996). On the solution of population balance equations by discretization – I. A fixed pivot technique. *Chemical Engineering Science*, **51**, 1311-1332.

Liao, Y., Lucas, D., (2009). A literature review of theoretical models for drop and bubble breakup in turbulent dispersions. *Chemical Engineering Science*, **64**, 3389-3406

Liao, Y., Lucas, D., (2010). A literature review on mechanisms and models of the coalescence process of fluid particles. *Chemical Engineering Science*, **65**, 2851-2864

Liao, Y., Lucas, D., Krepper, E., (2014). Application of new closure models for bubble coalescence and breakup to steam-water vertical pipe flow. *Nuclear Engineering and Design*, **279**, 126-136.

Liao, Y., Rzehak, R., Lucas, D., Krepper, E., (2015). Baseline closure model for dispersed bubbly flow: bubble coalescence and breakup. *Chemical Engineering Science*, **122**, 336-349.

Liao, Y., Lucas, D., (2016). Poly-disperse simulation of condensing steam-water flow inside a large vertical pipe. *International Journal of Thermal Sciences*, **104**, 194-207.

Liao, Y., Oertel, R., Kriebitzsch, S., Schlegel, F., Lucas, D., (2018). A discrete population balance equation for binary breakage. *International Journal of Numerical Methods in Fluids*, DOI: 10.1002/fld.4491.

Liao, Y., Lucas, D., (2018). Evaluation of interfacial heat transfer models for flashing flow with two-fluid CFD. *Fluids 2018*, **3**, 38; doi:10.3390/fluids3020038.

Liao, Y., Ma, T., Krepper, E., Lucas, D., Fröhlich, J., (2019). Application of a novel model for bubble-induced turbulence to bubbly flows in containers and vertical pipes. *Chemical Engineering Science*, **202**, 55-69.

Lifante, C., Frank, T., Burns, A.D., Lucas, D., Krepper, E., (2010). Prediction of polydiserse steam bubble condensation in sub-cooled water using the inhomogeneous MUSIG model. *7th International Conference on Multiphase Flow*, ICMF 2010, Tampa, FL USA, May 30-June 4, 2010.

Lo, S., Zhang, D., (2000). Application of population balance to CFD modelling of gas-liquid reactors. *Proceedings of Trends in Numerical and Physical Modelling for Industrial Multiphase Flows*, Corse, 27-29 September 2000.

Lucas, D., Krepper, E., Prasser, H.-M., (2005). Development of co-current air-water flow in a vertical pipe. *International Journal of Multiphase Flow*, **31**, 1304-1328.

Lucas, D., Frank, T., Lifante, C, Zwart, P., Burns, A. (2011). Extension of the inhomogeneous MUSIG model for bubble condensation. *Nuclear Engineering and Design*, **241**, 4359-4367.

Lucas, D., Rzehak, R., Krepper, E., Ziegenhein, T., Liao, Y., Kriebitzsch, S., Apanasevich, P., (2016). A strategy for the qualification of multi-fluid approaches for nuclear reactor safety. *Nuclear Engineering and Design*, **299**, 2-11.

Luo, H., Svendsen, H.F., (1996). Theoretical model for drop and bubble breakup in turbulent dispersions. *AIChE Journal*, **42**, 1225-1233.

Ma, T., Santarelli, C., Ziegenhein, T., Lucas, D., Fröhlich, J., (2017). Direct numerical simulation-based Reynolds-averaged closure for bubble-induced turbulence. *Physical Review Fluids*, **2**, 034301.

Menter, F. R., (1994). Two-equation eddy-viscosity turbulence models for engineering applications. *AIAA-Journal*, **32**, 1598-1605.

Metzger, L., Kind, M., (2017). The influence of mixing on fast precipitation processes – A coupled 3D CFD-PBE approach using the direct quadrature method of moments (DQMOM). *Chemical Engineering Science*, **169**, 284-298.

Min, J., Bao, Y., Chen, L., Gao, Z., Smith, J.M., (2008). Numerical simulation of gas dispersion in an aerated stirred reactor with multiple impellers. *Industrial Engineering Chemical Research*, **47**, 7112-7117.

Prince, M.J., Blanch, H.W., (1990). Bubble coalescence and break-up in air-sparged bubble columns. *AIChE Journal*, **36**, 1485-1499.

Ramkrishna, D. (1985). The status of population balances. *Reviews in Chemical Engineering*, **3**, 49-95.

Ramkrishna, D. (2000). Population balances: Theory and applications to particulate systems in engineering. Academic Press, 2000.

Scott, W.T., (1968). Analytic studies of cloud droplet coalescence I. *Journal of the Atmospheric Sciences*, **25**, 54-65.

Sun, X., Kim, S., Ishii, M., Beus, S.G., (2004). Modeling of bubble coalescence and disintegration in confined upward two-phase flow. *Nuclear Engineering and Design*, **230**, 3-26.

Tomiyama, A., Tamai, H., Zun, I., Hosokawa, S., (2002). Transverse migration of single bubbles in simple shear flows. *Chemical Engineering Science*, **57**, 1849 – 1858.

Yeoh, G.H., Tu, J.Y., (2004). Population balance modelling for bubbly flows with heat and mass transfer. *Chemical Engineering Science*, **59**, 3125-3139.